11^{th} International Conference on Fracture Mechanics of Concrete and Concrete Structures
FraMCoS-11
J. M. Chandra Kishen, A. Ramaswamy, S. Ray and R. Vidyasagar (Eds)
https://doi.org/10.21012/FC11.092364

AXIAL MODE I CRACKING IN CORE REGIONS OF COMPRESSED REINFORCED CONCRETE COLUMNS SUBJECTED TO FIRE LOADING

Maximilian Sorgner*, Rodrigo Díaz Flores*, Hui Wang†, Christian Hellmich*, and Bernhard L.A. Pichler*

*Institute for Mechanics of Materials and Structures, TU Wien (Vienna University of Technology)
Vienna, Austria, European Union
e-mail: Bernhard.Pichler@tuwien.ac.at

†School of Naval Architecture, Ocean and Civil Engineering, Shanghai Jiao Tong University
Shanghai, China

Key words: fire loaded cylindrical columns, thermal eigenstrains, hindered-warping induced stresses, axial elongation constraint

Abstract. Reinforced concrete columns must withstand extreme scenarios like fires. Understanding their structural behavior during such events is of great interest to structural engineers. The present study is focused on a cylindrical reinforced concrete column subjected to a moderate fire. The analysis combines a Fourier series solution for radial heat ingress into the column and thermo-elastic Bernoulli-Euler beam theory. A temperature history known to be relevant for fire accidents is imposed as boundary condition at the lateral surface of the column. The resulting radial symmetric temperature field is translated into a field of thermal eigenstrains. The latter is decomposed, in every cross-section, into two portions: a spatially uniform portion representing the eigenstretch of the axis of the column, and a spatially nonlinear portion representing the eigenwarping of the cross-sections. The eigenstretch is constrained by the support conditions at the structural scale ("axial elongation constraint"). The eigenwarping is hindered, because the the cross-sections remain plane also in the deformed configuration. This activates hindered-warping-induced cross-sectional stresses which are self-balanced and, therefore, do not contribute to the normal force. Total thermal stresses are obtained from adding the hindered-warping-induced stresses to the normal-force-related stresses. The influence of the axial elongation constraint on the structural behavior is discussed in the context of a sensitivity analysis. Thereby, the compliance of a spring placed on top of the column is varied. The simulations are first performed under consideration of linear-elastic material behavior of steel and concrete. Subsequently, the analysis is extended towards consideration of elasto-brittle material behavior of concrete. It is concluded that the axial elongation constraint significantly influences the structural behavior and the mechanism of damage of the fire-loaded column. For small values of the constraint, concrete will crack in the core of the cross-section, due to tensile stresses reaching the tensile strength. For large values of the constraint, compressive stresses increase particularly close to the heated surface. This may lead to spalling provided that the stresses reach the compressive strength of concrete.

1 Introduction

Fire scenarios are a challenge when it comes to the design and the maintenance of reinforced concrete (RC) structures. Much research in this area has been focused on experimental campaigns where temperatures and displacements were measured throughout severe fire loading, see e.g. [3, 4, 8]. In addition to structural fire experiments, the Finite Element Method (FEM) has been used to simulate such tests, see e.g. [1, 3, 9], providing valuable insight into stress and strain distributions. Díaz et al. [2] analyzed tension-induced damage of a reinforced concrete frame structure within the first 30 minutes of its exposure to a moderate fire, using non-linear 3D FEM analyses. However, FEM approaches demand fine discretizations and, therefore, large computational efforts in order to obtain reliable results.

Sorgner et al. [13] analyzed the problem studied in [2] with the aim to significantly reduce the computational expenses while still providing a reliable insight into the behavior of the structure. This was achieved through engineering model reduction. The heat conduction problem was solved by means of a Fourier series solution. The thermo-mechanical problem was solved by using Timoshenko beam theory. Accounting for elasto-brittle behavior of concrete, the cross-sectional properties of all structural elements were introduced as functions of evolving damage of concrete. The described engineering-mechanics approach allowed for accurately simulating tension-induced cracking in the core of compressed columns with *rectangular* cross-sections, while increasing the speed of the structural analysis, relative to the FEM, by a factor of 500.

In the present contribution, the approach of Sorgner et al. [12, 13] is followed in order to analyze the thermo-mechanical behavior of columns with *circular* cross-sections, subjected to lateral heating. Generalizing the analysis of [12, 13], the axial elongation constraint of the column is controlled by means of a linear spring with stiffness c, see Fig. 1. In the absence of bending, the thermally induced eigenstrains will be subdivided, in every cross-section, into a constant portion (= eigenstretch of the axis of the column) and the non-linear portion (= eigenwarping of the cross-sections), see also [10, 11, 14, 15].

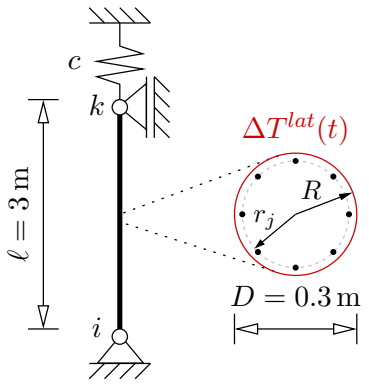

Figure 1: Idealized representation of the cylindrical column made from reinforced concrete: geometric and thermal boundary conditions and cross-sectional properties.

This paper is structured as follows. In Section 2, the heat conduction problem and the thermo-mechanical problem are solved for the case of circular reinforced concrete columns. In Section 3, the influence of the axial constraint of the columns on their cracking mechanism is investigated by performing a sensitivity analysis regarding the value of the stiffness of the linear spring. In Section 4, conclusions are drawn.

2 Thermo-mechanical analysis of a fire-loaded cylindrical RC column

A fire-loaded cylindrical column with a length of $\ell = 3\,\mathrm{m}$ and a radius of $R = 0.15\,\mathrm{m}$ is analyzed to identify the influence of the axial elongation constraint on the structural behavior of the column. It is made from reinforced concrete consisting of normal concrete "C40", with a mass-density amounting to $2373\,\mathrm{kg/m^3}$, and 8 steel rebars with a diameter of $d_s = 12\,\mathrm{mm}$, see Fig. 1. The thickness of the concrete cover amounts to $30\,\mathrm{mm}$. At its bottom, see node i in Fig. 1, the column is fixed to a pinned support. At the top of the column, see node k in Fig. 1, the horizontal displacement component and the bending moment are equal to zero, while the vertical displacement is constrained by means of a linear spring with stiffness c.

Thermo-mechanical properties of concrete and steel are listed in Table 1. Referring, strictly speaking, to room temperature, the listed values are also used at temperatures up to 200 °C.

Table 1: Thermo-mechanical properties of concrete (index c) and steel (index s), after [13].

Property	**concrete**	**steel**
Modulus of elasticity, E	$33.4\,\mathrm{GPa}$	$195\,\mathrm{GPa}$
Thermal expansion coefficient, α	$9.0 \times \frac{10^{-6}}{^\circ\mathrm{C}}$	$12.2 \times \frac{10^{-6}}{^\circ\mathrm{C}}$
Thermal diffusivity, a	$0.75\,\frac{\mathrm{mm}^2}{\mathrm{s}}$	$16.38\,\frac{\mathrm{mm}^2}{\mathrm{s}}$

A cylindrical r, φ, z-coordinate system is introduced. Its origin is located at node i. The z-coordinate runs upwards, following the axis of the column.

Cross-sectional properties are constant along the axial direction. The modulus of elasticity $E = E(r, \varphi)$ and the thermal expansion coefficient $\alpha = \alpha(r, \varphi)$ are considered to be heterogeneously distributed, see Fig. 1.

In the initial configuration, i.e. before the start of the fire, the temperature of the column is uniform (= reference temperature):

$$T_{ref} = 20\,^\circ\mathrm{C}\,. \tag{1}$$

The thermal loading is considered through a temperature evolution prescribed at the lateral surface of the column. This evolution is taken over from a large-scale fire test on a reinforced concrete frame structure consisting of slabs, walls, and columns, which was performed by Lu et al. [6]. The thermal loading of the test was defined based on a statistical analysis of documented fire accidents and a simulation performed by a fire dynamics simulation software. Thereby, automatic sprinkler devices, a ventilation system, and an energy release rate of the heat source of $5\,\mathrm{MW}$ were considered in order to simulate a scenario which is relevant for realistic fire accidents. The temperature history at the lateral surface of the columns was back-analyzed by Díaz et al. [2]. In the present study, the first $15\,\mathrm{minutes}$ of this temperature history are used as input, see Fig. 2.

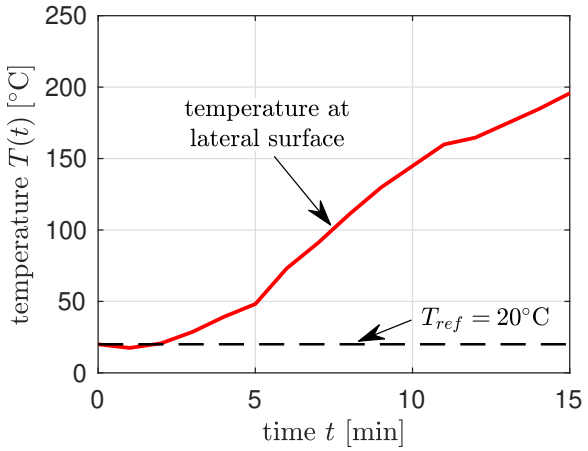

Figure 2: Thermal boundary condition: evolution of the temperature at the lateral surface of the column, after [6].

2.1 Solution of transient heat conduction in radial direction

Transient heat conduction is a boundary value problem. For thermally-isotropic media, the heat equation referring to cylindrical coordinates reads as [7]

$$\frac{\partial T}{\partial t} = a\left(\frac{\partial^2 T}{\partial r^2} + \frac{1}{r}\frac{\partial T}{\partial r} + \frac{1}{r^2}\frac{\partial^2 T}{\partial \varphi^2} + \frac{\partial^2 T}{\partial z^2}\right), \tag{2}$$

where T denotes the temperature, a the thermal diffusivity, and t the time variable.

The solution of the spatio-temporal problem described by Eq. (2) requires initial and boundary conditions. At the start of the fire, the temperature inside the column is uniform, see Eq. (1). As boundary condition, the temperature history at the lateral surface of the column is prescribed as illustrated in Fig. 2. Consequently, heat is conducted in radial direction. In other words, the temperature field does not depend on φ and z, and the heat equation (2) degenerates to

$$\frac{\partial T}{\partial t} = a\left(\frac{\partial^2 T}{\partial r^2} + \frac{1}{r}\frac{\partial T}{\partial r}\right), \tag{3}$$

where the temperature field is a function of the radial coordinate and the time, i.e. $T = T(r, t)$.

Given the linearity of Eq. (3), the superposition principle is applicable. This implies that the time-dependent boundary condition can be prescribed in a step-wise fashion. For each time step k, the temperature increment reads as

$$\Delta T_k^s = T^s(t_k) - T^s(t_{k-1}),\ \forall\, k \in [1;15]\,, \quad (4)$$

where the time difference $t_k - t_{k-1}$ amounts to $1\,\mathrm{min}$. The elementary solutions obtained for each temperature increment ΔT_k are superimposed to an analytical solution in series-developed form:

$$T(r,t) = T^s(t) - 2\sum_{k=1}^{15}\Delta T_k^s \sum_{n=1}^{\infty}\frac{J_0(\beta_n \frac{r}{R})}{J_1(\beta_n)\,\beta_n} \exp\left(-\frac{\beta_n^2}{R^2}a\langle t - t_k\rangle\right), \quad (5)$$

where $T^s(t)$ is the temperature at the lateral surface at time t, J_0 and J_1 the zeroth- and first-order Bessel functions of the first kind, respectively, β_n are the eigenvalues of the general zeroth-order Bessel function of the first kind, R denotes the radius of the column, and the angled brackets denote the Macauley operator: $\langle t - t_k\rangle := \frac{1}{2}\,(t - t_k + |t - t_k|)$.

The temperature field $15\,\mathrm{min}$ after the start of the fire is computed according to Eq. (5). Steps of surface temperature are considered every minute. These steps are quantified from Fig. 2. The thermal diffusivity of concrete is taken from Table 1. The thermal diffusivity of steel is set equal to that of concrete. This is reasonable, because the rebars have no significant influence on the heat conduction problem [5].

As a consequence of the first $15\,\mathrm{minutes}$ of fire loading, the temperature increases at the lateral surface of the columns to about $190\,^\circ\mathrm{C}$, and the heat front propagates by some $75\,\mathrm{mm}$ into the column, see Fig. 3 and Fig. 4. Thus, the temperature at the core of the column is still equal to the initial reference temperature.

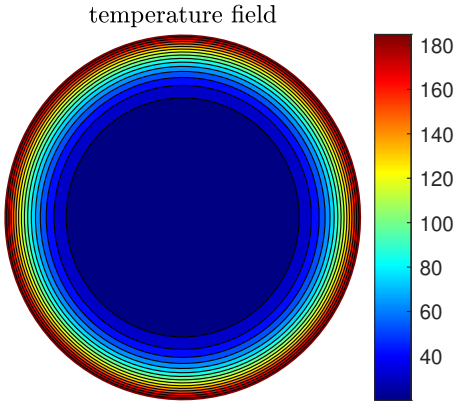

Figure 3: Temperature field obtained $15\,\mathrm{min}$ after the start of the fire.

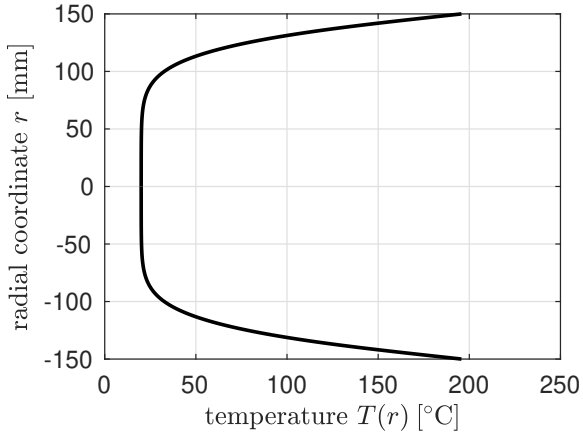

Figure 4: Temperature profile obtained $15\,\mathrm{min}$ after the start of the fire.

2.2 Decomposition of thermal eigenstrains

Thermal eigenstrains are proportional to the change of temperature, which is quantified relative to the reference temperature,

$$\Delta T = T - T_{ref}\,, \quad (6)$$

and the proportionality factor is the coefficient of thermal expansion α:

$$\varepsilon^e_{rr} = \varepsilon^e_{\varphi\varphi} = \varepsilon^e_{zz} = \alpha\,\Delta T\,, \quad (7)$$

As for the here-analyzed cylindrical columns, subjected to symmetric radial heat ingress, the thermal loading does not activate bending. Therefore, Bernoulli's hypothesis which states that the initially plane cross-sections remain

plane also in the deformed configuration, simply reads as

$$w(r, \varphi, z; t) = w_0(z; t)\,, \tag{8}$$

where w denotes the axial displacement field and w_0 the axial displacement component at the center of gravity of every cross-section.

The axial normal stress component σ_{zz} is obtained from inserting the definition of the axial normal strain component ε_{zz} of the linearized strain tensor, $\varepsilon_{zz} = \partial w/\partial z$, into the thermo-elastic version of Hooke's law, $\sigma_{zz} = E\,(\varepsilon_{zz} - \varepsilon^e_{zz})$. This yields, under consideration of Eq. (7)

$$\sigma_{zz} = E\left(\frac{\partial w}{\partial z} - \alpha\Delta T\right), \tag{9}$$

where E denotes the modulus of elasticity.

The constitutive law for the normal force N is obtained from inserting σ_{zz} according to Eq. (9) into the $N = \int_A \sigma_{xx}\,\mathrm{d}A$. This yields under consideration of Eqs. (7) and (8):

$$N = \overline{EA}\,(\varepsilon_0 - \varepsilon^e_0)\,, \tag{10}$$

with the extensional stiffness of the column reading as

$$\overline{EA} = \int_A E\,\mathrm{d}A\,, \tag{11}$$

the stretch of the axis of the column as

$$\varepsilon_0 = \frac{\partial w_0}{\partial z}\,, \tag{12}$$

and the eigenstretch of the axis of the column as

$$\varepsilon^e_0 = \frac{1}{\overline{EA}} \int_A E\,\alpha\Delta T\,\mathrm{d}A\,, \tag{13}$$

while A denotes the cross-sectional area.

An equation expressing the axial normal stresses σ_{zz} as a function of the normal force N follows from solving Eq. (10) for ε_0, from inserting this expression into Eq. (12), and of the resulting expression for $\partial w/\partial z$ into Eq. (9) as:

$$\sigma_{zz} = \frac{N\,E}{\overline{EA}} - E\,(\alpha\Delta T - \varepsilon^e_0)\,. \tag{14}$$

The strain in the brackets of Eq. (14) denotes the eigenwarping of the cross-sections, ε^e_w

$$\varepsilon^e_w = \alpha\Delta T - \varepsilon^e_0\,. \tag{15}$$

Solving Eq. (15) for $\alpha\Delta T$ delivers the sought decomposition of the thermal eigenstrains:

$$\alpha\Delta T(r, t) = \varepsilon^e_0(t) + \varepsilon^e_w(r, t)\,. \tag{16}$$

Eq. (16) states that the cross-sectional distribution of the thermal eigenstrain field, $\alpha\Delta T$, is decomposed into (i) a spatially uniform portion ε^e_0, see the eigenstretch of the axis of the column according to Eq. (13), and (ii) a spatially nonlinear rest ε^e_w, see the eigenwarping of the cross-sections according to Eq. (15).

The eigenstretch ε^e_0 is *free* to develop provided that the spring stiffness vanishes, $c = 0$, it is *constrained* provided that $0 < c < \infty$, and it is *hindered* provided that $c = \infty$. The eigenwarping is always hindered at cross-sectional scale, because the cross-sections remain plane even under thermo-mechanical loading [13].

2.3 Specific expressions for reinforced concrete columns

Specializing the effective extensional stiffness according to Eq. (11) for a reinforced concrete cross-section, consisting of concrete (index c) and steel rebars (index s), yields

$$\overline{EA} = E_c\Big[A_c + n_E\,A_s\Big] = E_c\,A_{eq}\,, \tag{17}$$

where A_c and A_s denote the cross-sectional subareas occupied by concrete and steel, respectively, $n_E = E_s/E_c$ denotes the ratio of the moduli of elasticity of steel E_s and concrete E_c, and A_{eq} denotes the "equivalent" cross-sectional area, see also Tables 1 and 2.

The eigenstretch of the reinforced concrete cross-section can be evaluated according to Eq. (13), under consideration of Eq. (17) and the thermal expansion coefficients of concrete and steel α_c and α_s, respectively, as

$$\varepsilon^e_0 = \frac{1}{A_{eq}}\left[\int_{A_c} \alpha_c\,\Delta T\,\mathrm{d}A + n_E \sum_{j=1}^{L} \alpha_s\,\Delta T_j\,A_j\right], \tag{18}$$

Table 2: Numerical values of cross-sectional properties.

cross-sectional area of concrete	$A_c = 70572.7\,\mathrm{mm}^2$
cross-sectional area of steel rebars	$A_s = 904.8\,\mathrm{mm}^2$
equivalent cross-sectional area of concrete	$A_{eq} = 95\,\mathrm{mm}^2$
ratio of the moduli of elasticity	$n_E = 5.838$

where L stands for the number of rebars, ΔT_j for the temperature change experienced by the j^{th} rebar, and A_j for its cross-sectional area.

The eigenstretch of the reinforced concrete column can be expressed as a function of the surface temperature history by inserting the temperature change according to Eqs. (5) and (6), into Eq. (18) as

$$\varepsilon_0^e = \alpha_c \frac{A_c}{A_{eq}} \left[\Delta T^s - 4 \sum_{k=1}^{15} \Delta T_k^s \sum_{n=1}^{\infty} \frac{1}{\beta_n^2} \exp(-\frac{\beta_n^2}{R^2} a \langle t - t_k \rangle) \right] + n_E\, \alpha_s \sum_{j=1}^{L} \frac{A_j}{A_{eq}} \Delta T_j \,. \tag{19}$$

$15\,\mathrm{minutes}$ after the start of the analyzed fire, the eigenstretch amounts to

$$\varepsilon_0^e(t = 15\,\mathrm{min}) = 4.022 \times 10^{-4} \,. \tag{20}$$

The eigenwarping of the cross-section is computed by inserting the value of ε_0^e into Eq. (15).

A specific expression for the axial normal stresses is obtained from Eq. (14), under consideration of $\overline{EA}$ according to Eq. (17), as

$$\sigma_{zz,c} = \frac{N}{A_{eq}} + \sigma_{zz,c}^e \,, \tag{21}$$

$$\sigma_{zz,s} = \frac{N\, n_E}{A_{eq}} + \sigma_{zz,s}^e \,, \tag{22}$$

where the hindered-warping-induced stresses read as

$$\sigma_{zz,c}^e = -E_c \left(\alpha_c \Delta T - \varepsilon_0^e \right) , \tag{23}$$

$$\sigma_{zz,s}^e = -E_s \left(\alpha_s \Delta T - \varepsilon_0^e \right) . \tag{24}$$

The hindered-warping-induced stresses are computed by inserting the temperature field T from Eq. (5) into Eq. (6), and the result together with the corresponding value of ε_0^e, into Eq. (23), see Fig. 5.

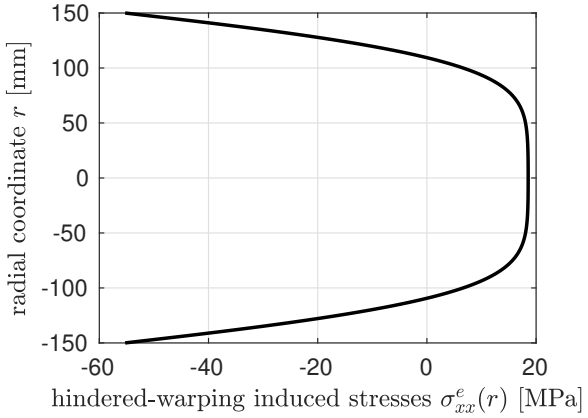

Figure 5: Hindered-warping-induced thermal stresses experienced by concrete, $15\,\mathrm{min}$ after the start of the fire.

The maximum hindered-warping-induced axial stress is tensile and amounts to $18.5\,\mathrm{MPa}$, which is larger than the tensile strength of concrete: $f_t = 3.5\,\mathrm{MPa}$. In order to find out whether or not these tensile stresses are compensated by normal-force-related stresses, the impact of the constraint of the eigenstretch on the normal force will be described next.

2.4 Normal force depending on the axial elongation constraint

In statically determinate columns, thermal eigenstretches are free to develop and do not activate internal forces. In statically indeterminate columns, in turn, the support conditions constrain the thermal eigenstretches. For the here-analyzed column, this constraint is modeled by a spring with stiffness c following a linear relation between the normal force of the column N and the axial displacement at node k, w_k, as

$$N = -c\, w_k \,. \tag{25}$$

The minus sign in Eq. (25) describes that an upward movement of node k of the column results in a compressive normal force.

The absolute value of the elongation of the axis of the column is equal to the absolute value

of the shortening of the spring. Under consideration of Eq. (25) and the length of the column ℓ, the axial stretch of the column reads as

$$\varepsilon_0 = \frac{w_k}{\ell} = -\frac{N}{c\,\ell}\,. \tag{26}$$

Notably, Eq. (26) implies that heating of the column, resulting in its expansion ($\varepsilon_0 > 0$), goes along with an upward movement of node k ($w_k > 0$) and a compressive normal force ($N < 0$).

An expression of the normal force as a function of the thermal eigenstretch of the axis of the column is obtained by insertion of Eq. (26) and (17) into Eq. (10), and by solving the resulting expression for N:

$$N = -\frac{\varepsilon_0^e}{\dfrac{1}{c\,\ell} + \dfrac{1}{E_c\,A_{eq}}}\,. \tag{27}$$

The normal force is equal to zero if the spring stiffness is equal to zero, i.e. if the thermal eigenstretch is free to develop. The normal force is equal to $-\varepsilon_0^e\,E_c\,A_{eq}$ if the spring stiffness approaches infinity, i.e. if the thermal eigenstretch is hindered.

The physical range of possible values of the spring stiffness, $0 < c < \infty$, provides the motivation to introduce a dimensionless spring compliance as

$$d = \frac{1}{1 + \dfrac{c\,\ell}{E_c\,A_{eq}}} \quad \in [0;1]\,. \tag{28}$$

The minimum stiffness, $c = 0$, refers to the maximum compliance, $d = 1$, and the maximum stiffness, $c = \infty$, refers to the minimum compliance, $d = 0$. The corresponding expression for the normal force as a function of d follows from Eqs. (27) and (28) as

$$N = -\,(1-d)\,\varepsilon_0^e\,E_c\,A_{eq}\,. \tag{29}$$

3 Results and discussion

3.1 Linear-elastic thermal stresses depending on the spring compliance

A sensitivity analysis regarding the axial elongation constraint is performed in order to analyze its influence on the structural behavior of the fire-loaded column. The problem is analyzed five times, whereby the level of the axial elongation constraint is varied by varying the value of the dimensionless spring compliance: $d \in [0, 0.25, 0.5, 0.75, 1]$, see Eq. (28). In all five cases, the same material properties are used, see Tables 1 and 2.

The temperature distribution inside the column (Fig. 3) as well as the thermal eigenstretch of the axis, obtained $15\,\mathrm{min}$ after the start of the fire, see Eq. (20), are independent of geometric boundary conditions of the column. Thus, the distribution of hindered-warping-induced stresses (Fig. 5) is valid for all five analyzed scenarios.

The normal forces are quantified by inserting the dimensionless spring compliance d as well as ε_0^e from Eq. (20), E_c from Table 1, and A_{eq} from Table 2 into Eq. (29), see Table 3.

Table 3: Absolute value of the normal force N depending on the dimensionless spring compliance d, see Eq. (29).

$d\,[-]$	0	0.25	0.5	0.75	1
$\lvert N\rvert\,[\mathrm{kN}]$	1007.5	756.4	504.2	252.1	0

Axial stresses experienced by concrete result from two contributions, see Eq. (21): (i) the compressive normal-force-related stresses depending on the axial elongation constraint, and (ii) the hindered-warping-induced stresses. Compressive normal-force-related stresses are uniformly distributed over the cross-section. Adding the hindered-warping-induced stresses leads to non-linearly distributed axial normal stresses, see Fig. 6.

For a dimensionless spring compliance equal to zero, i.e. when the thermal elongation is hindered ($d = 0 \Leftrightarrow c = \infty$), the axial stresses are compressive in the entire cross section. Tensile hindered-warping-induced stresses (Fig. 5) are overcompensated by compressive normal-force-related stresses. Small compressive stresses are obtained at the core of the column, but large compressive stresses in the near-surface region.

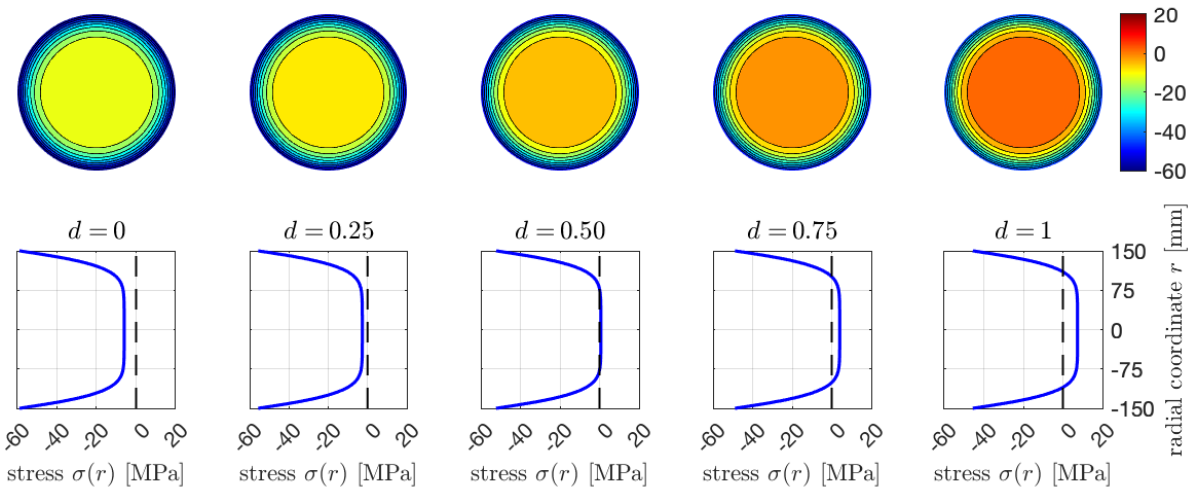

Figure 6: Stress profiles obtained 15 min after the start of the fire.

With increasing spring compliance, i.e. with decreasing axial elongation constraint, the normal-force-related stresses decrease. The total axial stresses shift towards tensile stresses. When d becomes equal to 1, i.e. when c becomes equal to 0, then N becomes equal to 0 and the axial normal stresses are equal to the hindered-warping-induced stresses, compare the rightmost diagram in Fig. 6 with Fig. 5.

The performed linear-elastic analysis provides realistic results for values of the dimensionless spring compliance smaller than 0.71. For larger values, the obtained tensile stresses are, at least along the axis of the column, larger than the tensile strength of concrete, see the stress profiles for $d = \{0.75, 1\}$ in Fig. 6. This unrealistic results provide the motivation to extend the model towards consideration of tensile failure of concrete.

3.2 Elasto-brittle modeling of tensile cracking in the core of a cylindrical column

Brittle tensile failure of concrete in form of tension-induced cracking, is modeled by introducing circular cross-sectional cracks with radius R^{cr}. The axial spacing between neighboring cracks is assumed to be sufficiently small, preventing the activation of significant concrete stresses in between the cracks [13]. The effective extensional stiffness (17) will be reduced for all cross-sections along the entire length of the columns, ensuring that the updated values are representative for cracked cross-sections.

The temperature field inside the column (Fig. 3) and the distribution of thermal eigenstrains remain valid for the elasto-brittle analysis, as heat conduction in radial direction is not affected by cracking. However, eigenstrains are now free to develop in the cracked core region. They remain constrained in the intact outer part of the column only. There, they are subdivided into an eigenstretch of the partly cracked column and an eigenwarping of the intact outer part of the cross-section.

The eigenstretch of the cracked column is computed similarly to the uncracked case: Insertion of the temperature difference obtained from Eqs. (5) and (6), into Eq. (18), while limiting the integration over the outer intact cross-sectional area, yields

$$\varepsilon_0^{cr} = \alpha_c \frac{1}{A_{eq}^{cr}} \Bigg[A_c^{cr}\,\Delta T^s - 4\,A_c \sum_{k=1}^{15} \Delta T_k^s \sum_{n=1}^{\infty} \frac{1}{\beta_n^2} \left(1 - \frac{R^{cr}}{R} \frac{J_1\left(\beta_n \frac{R^{cr}}{R}\right)}{J_1\left(\beta_n\right)} \right) \exp\left(-\frac{\beta_n^2}{R^2} a \langle t - t_k \rangle\right) \Bigg] + n_E\,\alpha_s \sum_{j=1}^{L} \frac{A_j}{A_{eq}^{cr}} \Delta T_j \,. \tag{30}$$

where the superscript cr stands for "cracked".

$A_{eq}^{cr} = A_{eq} - (R^{cr})^2\pi$ denotes the equivalent cross-sectional area of the intact part of the cross-section, and $A_c^{cr} = A_c - (R^{cr})^2\pi$ the intact cross-sectional area of concrete.

The eigenwarping of the cracked column is hindered at the intact outer part of the cross-section because it remains plane according to Bernoulli's hypothesis. Corresponding hindered-warping-induced stresses are computed by inserting the temperature difference ΔT obtained from Eqs. (5) and (6), and the value of the eigenstretch obtained from Eq. (30), into Eq. (23).

Total thermal stresses are computed iteratively, because the value of the crack radius, R^{cr}, is initially unknown. It is gradually increased in small steps until the thermal stresses obtained at the contour of the crack are equal to the tensile strength of concrete. Numerical values of the crack radius and the normal force of the column are listed in Table 4.

Table 4: Numerical value of the crack radius R^{cr} and the absolute normal force N, for spring compliance $d = \{0.75, 1\}$, obtained 15 min after the start of the fire.

d	0.75	1
R^{cr}	116 mm	129 mm
$\|N\|$	220.9 kN	0 kN

During the first 11 min after the start of the fire, the total thermal stresses in both columns are smaller than the tensile strength of concrete. After 12 min of heating, the tensile strength is reached at the axis of the column with spring compliance $d = 1$, while the tensile strength at the axis of the column with spring compliance $d = 0.75$, is reached after 14.6 min. Cracks propagate very fast from the time instant of crack initiation, which can be explained from the almost uniform stress state at the central region, caused from slow heat ingress into the columns, see Fig. 6. 15 min after the start of the fire, the cracks have extended across 60% and 73% of the total cross-sectional area, respectively, see Fig. 7. With increasing dimensionless spring compliance, i.e. with decreasing axial elongation constraint, the time of crack initiation decreases. Cracking leads to reduced compressive stresses in the near-surface region, triggered by stress redistributions from the inner cracked part of the cross-sections to the outer intact part.

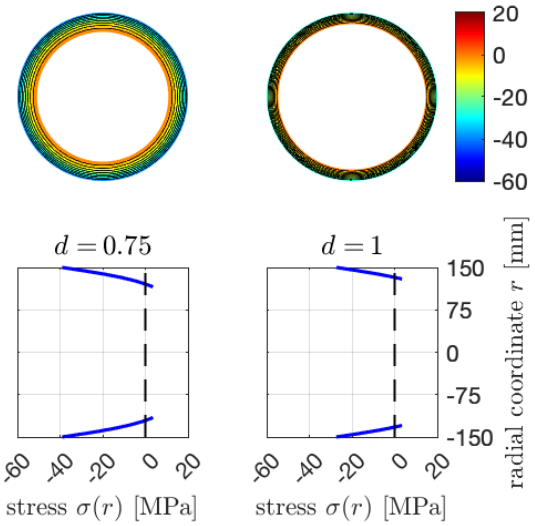

Figure 7: Stress profiles of cracked columns obtained 15 min after the start of the fire.

4 Conclusions

From the results of the presented study, it is concluded that the axial elongation constraint significantly influences the mechanism of deterioration of fire-loaded columns:

- For low levels of the axial elongation constraint, concrete will crack due to tensile stresses in the core region of the column, because tensile hindered-warping-induced stresses become the dominant contribution to the total thermal stresses in the core region.
- For high levels of the axial elongation constraint, compressive stresses rise in the near-surface region to values which are of the order of magnitude of the compressive strength of concrete. This can potentially lead to compressive failure, such as spalling.

REFERENCES

[1] Bratina, S., Čas, B., Saje, M. and Planinc, I. 2005. Numerical modelling of behaviour of reinforced concrete columns in

fire and comparison with Eurocode 2. *International Journal of Solids and Structures* **42**; 5715-5733.

[2] Díaz Flores, R., Wang, H., Mang, H., Yuan, Y. and Pichler, B.L.A. 2018. Numerical analysis of a moderate fire inside a segment of a subway station. *Applied Siences* **8**:2116.

[3] Gao, W., Dai, J.G., Teng, J. and Chen, G. 2013. Finite element modeling of reinforced concrete beams exposed to fire. *Engineering Structures* **52**; 488-501.

[4] Kodur, V., Raut, N., Mao, X. and Khaliq, W. 2013. Simplified approach for evaluating residual strength of fire-exposed reinforced concrete columns. *Material and Structures* **46**; 2059-2075.

[5] Lie, T. and Erwin, R. 1993. Method to calculate the fire resistance of reinforced concrete columns with rectangular cross section. *ACI Structural Journal* **90**; 52-60.

[6] Lu, L., Qiu, J., Yuan, Y., Tao, J., Yu, H., Wang, H. and Mang, H. 2019. Large-scale test as the basis of investigating the fire-resistance of underground RC substructures. *Engineering Structures* **178**; 12-23.

[7] Özisik, M.N. 1993. Heat Conduction. *John Wiley & Sons*.

[8] Ring, T., Zeiml, M. and Lackner, R. 2014a. Underground concrete frame structures subjected to fire loading: Part I–large-scale fire tests. *Engineering Structures* **58**; 175-187.

[9] Ring, T., Zeiml, M. and Lackner, R. 2014b. Underground concrete frame structures subjected to fire loading: Part II–re-analysis of large-scale fire tests. *Engineering Structures* **58**; 188-196.

[10] Schmid, S.J., Díaz Flores, R., Aminbaghai, M., Eberhardsteiner, L., Wang, H., Blab, R. and Pichler, B.L.A. 2022. Significance of eigenstresses and curling stresses for total thermal stresses in a concrete slab, as a function of subgrade stiffness. *International Journal of Pavement Engineering*, 1-17.

[11] Schmid, S.J., Díaz Flores, R., Aminbaghai, M., Pichler, B.L.A., Eberhardsteiner, L., Blab, R. and Wang, H. 2022. Curling stresses and thermal eigenstresses in a concrete pavement slab, in: *Computational Modelling of Concrete and Concrete Structures*; 564-571.

[12] Sorgner, M., Díaz Flores, R., Wang, H. and Pichler, B.L.A. 2022. Engineering Mechanics Analysis of a Moderate Fire Inside a Segment of a Subway Station, in: *Proceedings of the Conference on Computational Modelling of Concrete and Concrete Structures (EURO-C 2022)*; 239-246.

[13] Sorgner, M., Díaz Flores, R., Wang, H., Hellmich, C. and Pichler, B.L.A. 2023. Hindered thermal warping triggers tensile cracking in the cores of compressed columns of a fire-loaded tunnel segment structure: efficiency and accuracy of beam theory prediction, compared to FEM. *Applications in Engineering Science* **14**:100128.

[14] Wang, H., Höller, R., Aminbaghai, M., Hellmich, C., Yuan, Y., Mang, H.A. and Pichler, B.L.A. 2019. Concrete pavements subjected to hail showers: A semi-analytical thermo-elastic multiscale analysis. *Engineering Structures* **200**:109677.

[15] Wang, H., Yuan, Y., Mang, H.A., Ai, Q., Huang, X. and Pichler, B.L.A. 2022. Thermal stresses in rectangular concrete beams, resulting from constraints at microstructure, cross-section, and supports. *European Journal of Mechanics-A/Solids* **93**:104495.